Analysis of floating and end-bearing pile foundations affected by deep-excavations

Article *in* Computers and Geotechnics · January 2023

DOI: 10.1016/j.compgeo.2022.105075

CITATION
1

READS
186

3 authors, including:

Chen Zheng
Universidad Politécnica de Madrid
8 PUBLICATIONS **33** CITATIONS
SEE PROFILE

Andrea Franza
Aarhus University
80 PUBLICATIONS **739** CITATIONS
SEE PROFILE

Computers and Geotechnics 153 (2023) 105075

Contents lists available at ScienceDirect

Computers and Geotechnics

journal homepage: www.elsevier.com/locate/compgeo

Research paper

Analysis of floating and end-bearing pile foundations affected by deep-excavations

Chen Zheng [a], Andrea Franza [b,*], Rafael Jimenez [a]

[a] ETSI Caminos, Canales y Puertos, Universidad Politécnica de Madrid, Madrid, Spain
[b] Department of Civil and Architectural Engineering, Aarhus University, Aarhus, Denmark

ARTICLE INFO

Keywords:
Deep-excavations
Soil movements
Piles
Soil–structure interaction
Layered soil
Building deformations

ABSTRACT

This paper investigates the response of pile foundations to deep-excavations. An elastoplastic two-stage model is used to study the response of pile groups (with free- or rigidly capped-heads) and of piled structures (grade beams or bearing walls), considering piles embedded in either uniform or layered ground. The model is validated using results of analytical solutions, as well as data from centrifuge tests and from real case histories. Then, a parametric study investigates excavation-induced displacements and internal forces of piles, and deformations of the superstructure. Soil–pile transfer mechanisms and pile–superstructure interactions are analysed for various foundations and ground conditions, with results showing that settlements and slopes between piles are larger for floating piles than for end-bearing piles. Results show that rigidly capped piles and semi-flexible piled structures cause bending moments at the foundation heads that increase with the excavation-induced slope between piles, whereas the risk for tensile failure of piles is low. Also, results indicate that the superstructure stiffness is more relevant to decrease the slope and deflection ratio of foundations when composed of floating piles, compared to end-bearing piles. Finally, modelling end-bearing piles embedded in a stiff base using hinged connections to such stiff base may not be appropriate.

1. Introduction

There is an increasing demand for *deep-excavations* (i.e., considered herein as vertical excavations requiring the support of a retaining wall, such as a diaphragm wall, that extends below the excavation bottom and that is constructed/installed prior to such excavation) for infrastructure development and the construction of new buildings, particularly in congested urban areas. As shown in Fig. 1a, the displacement of the retaining wall supporting a deep-excavation results inevitably in ground movements that can affect nearby piles and their superstructure. Thus, excavations can increase the deformation and loads of piles supporting nearby buildings or other infrastructure, hence leading to risks for their integrity (e.g., damage at pile head-to-cap connections) or to serviceability losses in the superstructure (e.g., cracking in non-structural infills). While pile distress can be evaluated directly from internal forces, displacements (maximum settlement) and deformation parameters (deflection ratio, bay slope) shown in Fig. 1 can be used to estimate serviceability losses in the superstructure.

Recent case histories illustrated the threat posed by deep–excavations conducted near piles and buildings. Excavation-induced lateral movements can result in large deflections of piles (Finno et al., 1991; Goh et al., 2003), while Tan et al. (2016) reported settlements of 40 mm for buildings founded on short piles adjacent to a subway station excavation. Also, Korff et al. (2016) monitored distortions of piled buildings due to excavation-induced settlements, while Finno and Bryson (2002) and Son and Cording (2005) demonstrated that excavation-induced settlements led to the cracking of bearing–walls and non–structural infills in buildings with shallow foundations. Although Goh and Mair (2014) indicated that the stiffness of a superstructure (e.g., building) founded on shallow foundations could decrease its distortion levels, there is a lack of studies that addressed the role of the (piled) building stiffness in the excavation–pile–structure interaction. Furthermore, for ultimate limit state assessments, the unlikely scenario of unexpected failure of the retaining wall bracing system, and the subsequent large ground movements, should also be considered by engineers (Tan et al., 2018). Hence, developing design methods to estimate the behaviour of single pile and pile groups next to deep-excavations is important for geotechnical engineers. Such design methods should account for (i) the depth of the retaining wall relative to the pile length and (ii) the distribution of soil resistance along the pile. For (i), 'relatively short piles' and 'relatively long piles' are associated with wall-to-pile lengths ratios of $H_w/L_p \geq 1$ and $H_w/L_p < 1$, respectively, as shown in Fig. 1a. Note that the wall depth H_w (rather than the excavation depth

* Corresponding author.
E-mail address: anfr@cae.au.dk (A. Franza).

https://doi.org/10.1016/j.compgeo.2022.105075
Received 28 January 2022; Received in revised form 4 October 2022; Accepted 5 October 2022
Available online 17 October 2022

Notation

b_b	Equivalent beam cross-sectional width
c_u	Undrained shear strength of soil
d_b	Equivalent beam cross-sectional depth
d_p	Pile diameter
ν_s	Poisson's ratio for soil
ν_p	Poisson's ratio of pile
ω_{max}	Maximum slope of the superstructure
q_b	Ultimate base stress
ρ_{hog}	Relative bending stiffness parameters
s_{max}	Maximum differential settlement in piled structure
s_p	Pile spacing
σ_h^{exc}	Excavation-induced horizontal pressure
σ_h^{pos}	Post-excavation horizontal pressure
τ	Shaft friction
τ^{pos}	Post-excavation shaft friction
τ_f	Shaft ultimate friction
u_x	Horizontal displacement of pile
u_x^{exc}	Excavation-induced horizontal displacement of pile
u_z	Vertical displacement
u_z^{exc}	Excavation-induced vertical displacement
x	Horizontal spatial coordinate
z	Depth, measured from ground surface
Δ_{hog}^{bldg}	Relative building deflection in hogging region
Δ_{hog}^{gf}	Relative greenfield deflection in hogging region
DR_{hog}^{bldg}	Deflection ratio in hogging region of the building
DR_{hog}^{gf}	Deflection ratio in hogging region of the greenfield settlement trough
EI	Bending stiffness of building
E_p	Young's modulus of pile
E_s	Young's modulus of soil
E_{ss}	Young's modulus of superstructure
H	Excavation depth
H_w	Wall length
L	Building width
L_e	Pile embedding depth
L_{hog}^{bldg}	Transverse length of hogging region of building settlement trough
L_{hog}^{gf}	Transverse length of hogging region of greenfield settlement trough
L_p	Pile length
M	Pile bending moment
M^{exc}	Excavation-induced bending moment
M_{hog}^{DR}	Modification factor in hogging region of building settlement trough
M^{pos}	Post-excavation bending moment
N	Axial force
N^{exc}	Excavation-induced axial force
N_b^{exc}	Excavation-induced base force
N^{pos}	Post-excavation axial force
N_{max}^{pos}	Maximum post-excavation axial force of pile in pile group
P_b	Pile base reaction load
P_0	Pre-excavation service load at the pile head
P_u	Ultimate horizontal pressures of soil
Q_b	Ultimate capacity of pile base
Q_r	Pile base capacity as a percentage of total capacity
$Q_{s,1}$	Ultimate capacity of pile shaft in the top layer
Q_{tot}	Maximum capacity of pile
SF_0	Initial safety factor
$S_{p,1}$	Pile space in pile group
$S_{p,2}$	Pile space in piled structure
$X_{p,1}$	Offset of the front pile
GF	Greenfield
EL	Elastic
EP	Elastoplastic
SP	Single pile
PG	Pile group
PS	Piled structure

H) is adopted in this paper to conduct the analyses and to identify relatively low and short piles; this is because typical excavation and support conditions frequently lead to similar excavation depths being associated with similar wall depths, while horizontal displacements also occur for the embedded part of the wall, hence making it a more relevant parameter to consider in our analyses. For (ii), piles can be considered within a range varying from 'floating piles' (i.e., piles entirely embedded in a relatively uniform soil, so that shaft resistance is dominant) to 'end-bearing piles' (i.e., with tips embedded in a deep stiff layer where most of the pile's load capacity is mobilised).

2. Background

In the last two decades, experimental evidence of the detrimental effects of deep-excavations on nearby pile foundations has been collected. Centrifuge testing has been used to evaluate the response of single piles (Leung et al., 2000, 2006; Ong et al., 2006) and of pile groups (Leung et al., 2003; Choudhury et al., 2008; Ong et al., 2009). All were 'end-bearing' piles with no applied working load and considered unsupported excavations in both soft clay and sand. These experimental results show that lateral deflections and bending moments of piles reduce considerably with their distance to the retaining wall. Also, the response of capped pile groups (in comparison to single piles) is characterised by lower maximum horizontal displacements of the front pile, close to the excavation, due to the restraining action of rear piles through the cap; however, this group response can lead to large bending moments at the pile–cap connection. Also, 'end-bearing' piles underwent in several cases horizontal movements larger than their settlements. On the other hand, pile settlements can be significant for 'floating' piles (Ng et al., 2017) and centrifuge tests of propped excavations next to a loaded 'floating' pile in uniform sand indicated that the pile head condition seems not to affect the pile settlement, whereas it significantly influences the bending moment in the upper part of the pile. Yet, there is a lack of understanding of piled structures affected by excavations.

Also, advanced numerical modelling has been limited to single piles and pile groups with a rigid cap. For instance, Liyanapathirana and Nishanthan (2016) parametrically studied the effects of excavations on the lateral response of single piles, concluding on the importance of excavation depth and pile head fixity on pile behaviour. Shakeel and Ng (2018) conducted 3D coupled consolidation analyses to gain insight into the axial and flexural response of pile groups embedded in uniform clays, displaying the importance of the relative location of the

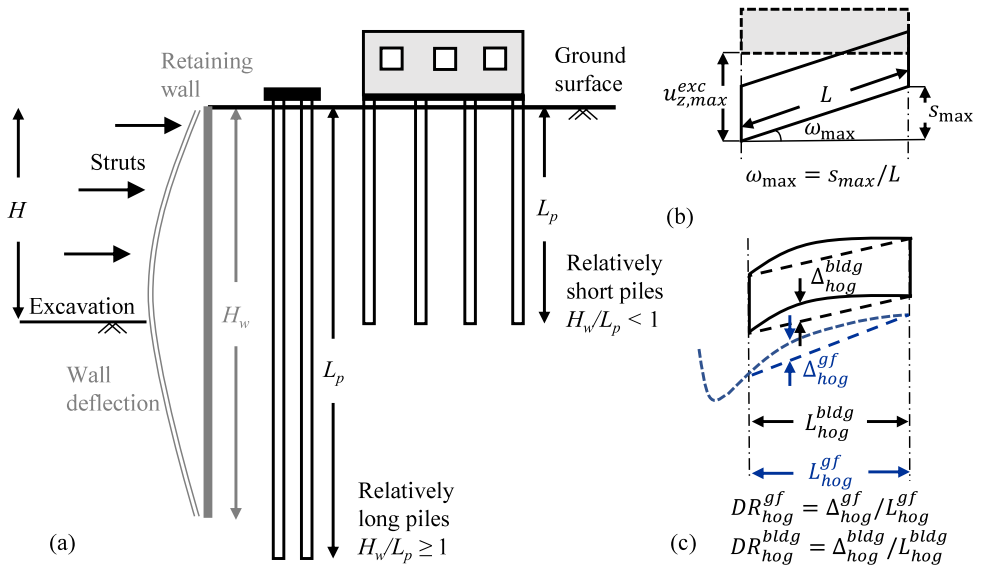

Fig. 1. (a) Problem of pile foundations adjacent to a deep-excavation; (b) maximum settlement and slope of the superstructure; (c) excavation-induced deflections of the superstructure.

pile toe in relation to the final excavation level. Pile groups experience higher settlement and tilting if the pile toes are located closer to the final excavation level, while a significantly higher bending moment is induced when the pile toes are located well below the final excavation level than when at the final excavation level. A similar parametric study in uniform clays was carried out by Soomro et al. (2019) for 'floating' single piles with constant head load, detailing the impact of displacement restraints of the pile head on bending movements and of working load level on settlements. The excellent agreement between numerical simulations and centrifuge tests also demonstrated that advanced numerical analyses could reliably model this problem. However, it also requires considerable computational and time efforts along with a careful choice of soil constitutive models. Therefore, it may not always be suitable during preliminary design stages or for sensitivity studies dealing with many excavation and support systems (and thus ground movement distributions) next to piled structures.

Experimental and numerical evidence suggests the importance of considering the stiffness of both the ground (that could be layered) and the structures above the piles (caps, grade beams/slabs, or the building), since they can significantly affect deformations and displacements of piles. For this, models capable of accounting for both excavation and superstructure effects, such as simplified two-stage interaction models, are needed. In these models, the greenfield soil movements (i.e. displacements in the absence of existing foundations near the deep-excavations) are estimated first; subsequently, the soil–pile–structure system is subjected to a set of 'active' external and live loads and, then, to equivalent 'passive' loads (the latter resulting in the greenfield movements when no foundation is present). To describe soil–pile and pile–soil–pile interactions, either the half-space theory (Poulos, 1989; Xu and Poulos, 2001) or the Pasternak/Winkler soil model (Kitiyodom et al., 2005; Huang et al., 2009; Zhang et al., 2011; Liu et al., 2020) may be used to capture the ground mass flexibility, while accounting for perfect compatibility or localised soil yielding in the near-pile region. Beam theory may be used to describe the structural response of piles. The condensed stiffness matrix approach can easily account for any structure (caps, frames, walls), when assumed linear elastic. Although two-stage methods have been extensively used to evaluate the effects of tunnelling on piles and pile groups (Chen et al., 1999; Loganathan et al., 2001; Franza et al., 2021a), previous applications to deep-excavation problems are mostly limited to single pile analyses: Poulos and Chen (1997) used a linear elastic boundary element model; Zhang et al. (2011) and Korff et al. (2016) proposed a Winkler-based analysis that considers nonlinear load transfer mechanisms between the pile and the soil. For pile groups, Liang et al. (2013) studied axially loaded pile groups subjected to lateral soil movement by using a Winker soil model for single piles and Mindlin's interaction factors for pile–soil–pile interactions. Mu et al. (2020) developed a two-stage method to predict the pile–raft (vertical and lateral) response due to deep-excavations, but the method is limited to elastic conditions. However, to the authors' knowledge, the coupled vertical and lateral response of pile foundations near to subsequent deep-excavations has not yet been investigated with elastoplastic two-stage models.

3. Scope

Considering the lack of a systematic study of excavation-induced effects on pile groups and piled structures in layered grounds, this paper aims to (i) evaluate the applicability of two-stage elastoplastic excavation–pile–structure interaction models (COMPILE Model) for this problem; and (ii) to characterise the influence of main input parameters on both types of foundations to deep-excavations in layered ground. First, the model was validated through comparison with BEM results, with experimental results and with data from relevant case histories. Next, parametric studies are conducted to investigate the effects of several aspects – wall depth, foundation geometry, structure and ground properties, etc. – on the excavation–pile–structure interaction response, with particular attention to induced displacements, pile structural distress, and structural deformations. Finally, the effect of the depth of embedding of 'end-bearing' piles into a stiffer deep layer is investigated. Considering the scope and limitations of the adopted model, findings are used to provide guidance to engineers on critical aspects to be considered during design of deep-excavations adjacent to existing deep foundations, rather than to quantify the effects of deep-excavations for specific cases or to provide design charts.

4. Elastoplastic interaction model

The three-dimensional two-stage model for excavation–soil–pile–structure interaction (Franza et al., 2021b) is adopted to investigate the effects of deep-excavations on piles and piled structures. In Stage 1 with active loads, the external and live actions are applied to the pile heads, and the foundation–structure system is solved for the *pre-excavation* state. Then, in Stage 2 with passive loads, the effects of excavation-induced greenfield movements on the foundation-structure system are

evaluated to compute *post-excavation* foundation displacements and internal forces. *Excavation-induced* displacements and internal forces are inferred from the variation between Stages 1 and 2.

4.1. Estimation of greenfield soil movements

Input soil movements describing the greenfield displacement field are either estimated from numerical modelling, experimental results, field information or computed analytically. In particular, for the parametric study in this paper, the superposition of singularities of cavity method is adopted, for which the deflection of the diaphragm wall is associated with a distributed ground loss is implemented as in Xu and Poulos (2000) and Zhang et al. (2011). Horizontal u_x^{GF} and vertical u_z^{GF} greenfield soil movements are obtained from Eq. (1) by integrating infinitesimal ground losses along the wall depth, using the displacement field of Sagaseta (1987) for point sinks in an incompressible half-space.

$$u_x^{GF} = \int_0^{H_w} \frac{2f(h)}{\pi} \left\{ -\frac{1}{2}\left(\frac{x}{r_1^2} - \frac{x}{r_2^2} \right) - \frac{x}{r_2^2}\left[1 - 2\frac{z(z+h)}{r_2^2} \right] \right\} dh$$
$$u_z^{GF} = \int_0^{H_w} \frac{2f(h)}{\pi} \left\{ -\frac{1}{2}\left(\frac{z-h}{r_1^2} - \frac{z+h}{r_2^2} \right) + \frac{z}{r_2^2}\left[1 - 2\frac{x^2}{r_2^2} \right] \right\} dh \quad (1)$$

where $r_1 = \sqrt{x^2+(z-h)^2}$; $r_2 = \sqrt{x^2+(z+h)^2}$; h is the integration variable; H_w is the diaphragm wall depth; x is the horizontal distance to the diaphragm wall; z is the depth to the ground surface; and $f(h)$ is the deflection of the diaphragm wall (i.e., its horizontal displacement profile). Although input greenfield displacements can be estimated numerically or analytically in plane-strain conditions, note that the COMPILE model solves the soil–pile-structure interaction as a three-dimensional boundary problem, as discussed later.

4.2. Analysis of soil–pile–structure interaction

The three-dimensional interaction model of Franza et al. (2021b), which was validated for tunnelling scenarios, is used. It assumes beams for the vertical piles, elastic isotropic half-space models for the soil (either uniform or layered), and localised soil yielding at the pile–soil interface. The structure consists of a rigid cap, a grade slab, or a masonry bearing wall, and all are modelled as a beam not in contact with the ground surface. From the half-space theory, the flexibility functions describing the relationship between the loads applied along the pile and the displacements of the half-space in the three spatial directions are obtained integrating the point–load solutions of Mindlin (1936) and Ai et al. (2002) along the pile boundary, hence overcoming limitations of Winkler models and interaction factors. It follows that the soil–pile and pile–soil–pile interaction mechanisms (along a given pile and between different piles) are linear elastic. This is a standard assumption in previous two-stage analyses, which has also been proved as reasonable in practice, based on case history and experimental data.

A perfectly-plastic interface, consisting of sliders, is interposed between the beam axis and the half-space to limit vertical and horizontal forces when ultimate shaft friction, base pressure, or lateral pressure are mobilised. These sliders capture, at a macro-scale, the effects of shear bands, slippage, or gap formation along the pile shaft and beneath its base. This localised plasticity approach for soil yielding along the pile is commonly adopted in foundation engineering (see e.g., Chow (1986) for vertical loads or Chen et al. (1999) for tunnelling). The limit forces of the vertical and horizontal sliders are defined by integrating the yielding stresses at the shaft and base: namely, negative and positive shaft friction, lateral shaft pressure, ultimate base pressure and no tensile capacity at the pile base. Importantly, differently for tunnelling in which lateral soil–pile interaction is mostly elastic (Basile, 2014), plastic sliders in the horizontal direction can play a role (as later discussed) because of possible large excavation-induced horizontal ground movements.

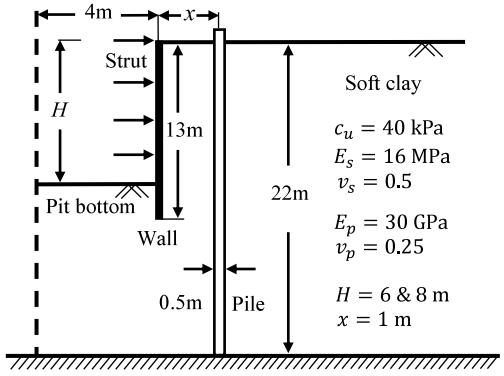

Fig. 2. Single pile adjacent to a deep-excavation considered by Poulos and Chen (1997).

The solution is obtained using the Finite Element Method approach, discretising the foundation in finite elements and computing the soil, foundation and superstructure matrices in correspondence with the nodal locations of the foundation. Linear elastic (EL) and elastoplastic (EP) analyses are performed: in the EL analyses, perfect compatibility is imposed between the pile and the continuum; in the EP analyses, the soil yielding at the pile–soil interface is considered by activating sliders. For further details of the model, refer to Franza et al. (2021b).

5. Model applicability to deep-excavations

The elastoplastic interaction model is validated by comparison with elastic Boundary Element Method (BEM) results (Poulos and Chen, 1997), centrifuge measurements (Ong et al., 2006, 2009) and field monitoring data (Korff et al., 2016) of deep-excavations.

5.1. Comparison with a linear elastic model (single pile)

The EL predictions of the proposed model are evaluated first using elastic BEM results of Poulos and Chen (1997) as a benchmark. Fig. 2 shows the considered scenario, consisting of a braced diaphragm wall of height H_w = 13 m next to a free-head, unloaded, 'end-bearing' single pile, with its shaft in soft clay and its base constrained by the rigid bedrock, with translations restricted and rotations allowed (the impact of the rotational constraint is investigated later). The pile has d_p = 0.5 m, L_p = 22 m; E_p = 30 GPa and its offset from the wall is 1 m. The clay has E_s = 16 MPa and ν_s = 0.5 (undrained). The input greenfield horizontal movements at the pile location are selected from plane-strain numerical simulations after (Poulos and Chen, 1997).

For the intermediate excavation depths of 6 m and 8 m, Fig. 3a shows the greenfield horizontal movements, while Fig. 3b and c compare the computed EL excavation-induced deflections (negative towards the excavation) and bending moments (negative when the tensile fibre is on the excavation side) of the pile against the BEM elastic results of Poulos and Chen (1997). Despite minor differences within the upper 5 m of the pile, the agreement between the two elastic models in terms of predicted pile deflection is excellent; the proposed model is capable of accounting for the complex distribution of bending moments and for the bedrock effect (no horizontal displacement of the base) thanks to the layered half-space theory adopted. As expected, the pile lateral movements and bending moments increase (more than twice) with the advancement of the excavation depth from 6 m to 8 m; interestingly, the bending moment distribution changes its shape, although the largest maximum bending moment is negative for both cases (with tensile fibre facing the excavation). Note that no bending moments are induced at the pile head due to the free-head conditions; this differs from capped or connected piles (as later discussed in the text).

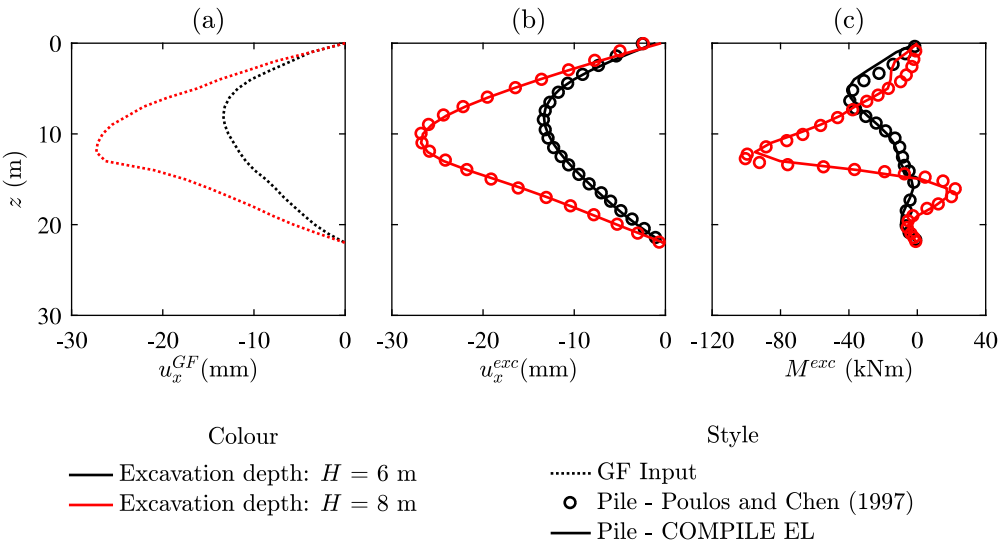

Fig. 3. Soil movements and pile response induced by the adjacent excavation: (a) greenfield and (b) pile horizontal displacements; (c) pile bending moments.

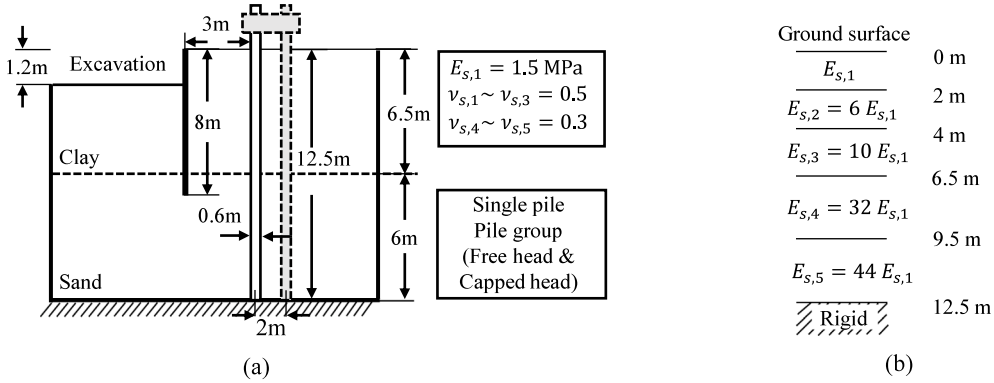

Fig. 4. (a) Centrifuge test configurations (Ong et al., 2006, 2009) (prototype scale). (b) Adopted ground model.

5.2. Comparison with centrifuge results (single pile and pile groups)

The reliability of the interaction model for excavations adjacent to piles is evaluated using centrifuge measurements from Ong et al. (2006, 2009), replicating a shallow excavation close to 'end-bearing' single piles and pile groups in layered ground.

Fig. 4 shows the scenarios modelled in the physical testing. The stratigraphy consists of a 6.5 m thick clay layer on top of a 6.0 m thick sand layer resting on a rigid base. For the overconsolidated but soft kaolin clay, the undrained shear strength c_u linearly increases from approximately 6 kPa to 10 kPa between depths of 2 m and 6.5 m; however, post-excavation strength dropped to 1 kPa for the top 2 m of soil (Ong et al., 2006). The 1.2 m excavation in clay is retained by a cantilever wall with a total height H_w of 8 m and with its tip reaching the underlying sand layer. Piles with length L_p = 12.5 m, diameter d_p = 0.6 m, and Young's modulus E_p = 35 GPa have their tip resting on the rigid base and they are located with their axes at either 3 m or 5 m offset from the wall, and with a spacing of 2 m within the 2 × 2 pile group.

To solve the excavation–pile interaction, horizontal movements measured at locations of pile axes during a greenfield test by Ong et al. (2006) were used as input, while greenfield settlements were neglected in these analyses. For the continuum ground model, five elastic layers were adopted, as shown in Fig. 4b, whose Young's moduli were estimated considering $E_s = 150c_u$ and $E_s = 6z$ for the clay and sand strata, respectively, where z is the depth from the surface to the mid-layer depth. Also, in the perfectly-plastic EP analyses, the ultimate horizontal pressures along the shaft in clay were taken as $P_u(z) = \min[2(1 + z/d_p)c_u, 9c_u]$ and the pile shaft resistance was assumed as $\tau_f = c_u$. For the ultimate horizontal pressures in sand, no yielding is assumed due to relatively large values of P_u.

Fig. 5a and b compare, for the model and the experimental data, the deflections and bending moments induced along the front single pile; the agreement is excellent, particularly when horizontal yielding is considered in the clay. To clarify the role of lateral soil yielding, Fig. 5c shows measured and calculated horizontal soil pressures acting on the pile. Soil pressures predicted by the EP model agree well with measured data at the top 7 m of the pile, despite minor differences along the bottom of the pile. Also, the interaction model captures the spike in the horizontal stresses at the clay–sand interface, which is typical in horizontal pile–soil interaction problems with a sudden change in ground stiffness (Ong et al., 2006).

Next, Fig. 6 shows the response of the pile groups to the excavation, when both free-head and rigidly capped-head conditions are tested. Fig. 6a displays that, for free-head conditions, the deflection of the front pile is greater than for the rear one so that, consequently, greater bending moments occur for the front free-head pile than for the rear one, as shown in Fig. 6b. On the other hand, this differential head deflection is prevented by the cap action in Fig. 6c, leading to a change in the curvature of the upper part of piles and, thus, to excavation-induced bending moments in the upper region of the piles. The agreement between both models is also good for the pile group case, with minor

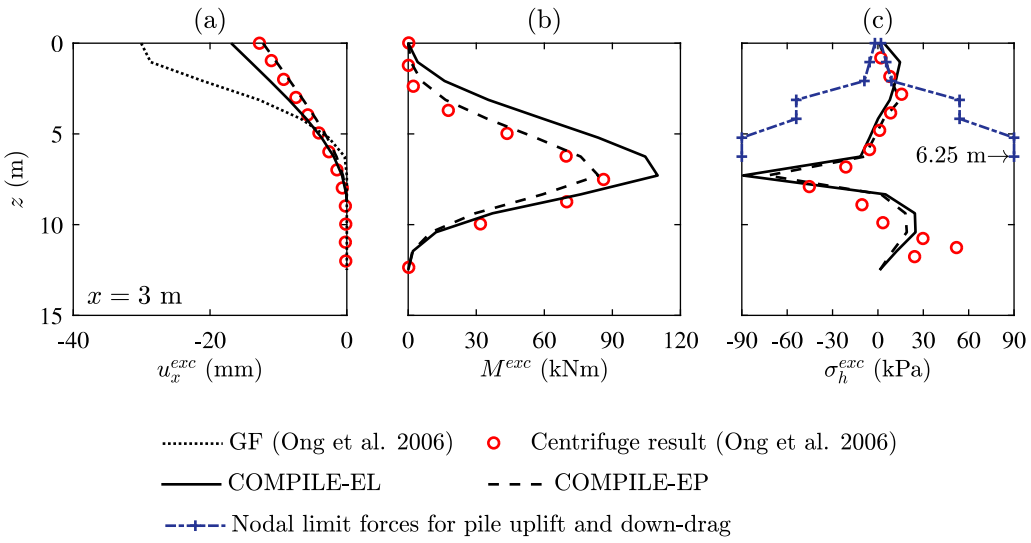

Fig. 5. Analyses of Ong et al. (2006, 2009) centrifuge test. Excavation effects on the single pile located 3 m behind wall: (a) lateral displacements, (b) bending moments, and (c) soil pressure.

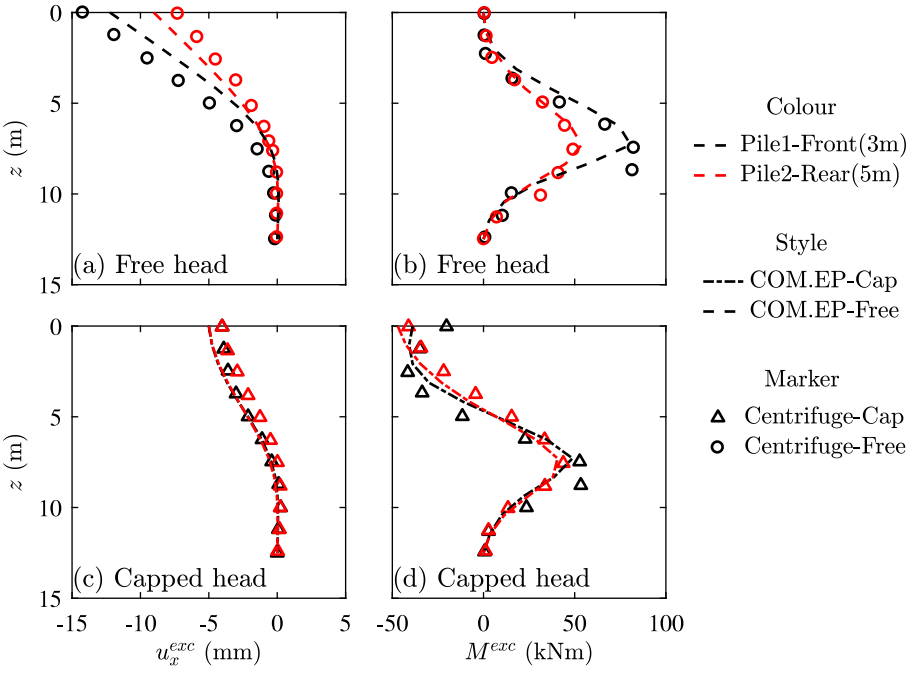

Fig. 6. Excavation effects on the pile groups: free-head (a)–(b) and (c)–(d) capped foundation.

differences only. The difference in the free-head deflections may be due to the greenfield soil input employed in the two-stage solution not being fully representative of the tests, which suffered large greenfield soil deformations (leading to surface displacements of 30 mm for a shallow excavation of 1.2 m); the difference in the bending moment for the capped case could be due to the rotational fixity being only partial in the experiments (Choudhury et al., 2008).

Centrifuge tests from Ong et al. (2006, 2009) —in which the offset from the retaining wall to the single pile or to the two-pile group was reduced from 3 m to 1 m— were also simulated; see supplemental data in Figures S1 and S2. The two-stage predictions also compared satisfactorily with the centrifuge results for this reduced (1 m) offset; this partly supports the model applicability under close spacing of piles and the retaining wall.

5.3. Comparison with field monitoring data (piled building)

In-situ measurements from Amsterdam (Korff, 2013; Korff and Mair, 2013b; Korff et al., 2016) are considered to evaluate the response of piled buildings to an excavation extending beneath their foundation level, as shown in Fig. 7. Settlement data of three-storey wall-bearing masonry buildings founded on wooden pile rows (so-called *Amsterdam foundation*) are available, which can be related to greenfield surface and subsurface ground movements. In particular, this paper focuses on Buildings 122, 124, and 126, adjacent to the excavation in a way such that they can be treated as a continuous façade (Korff, 2013). For these buildings, the thickness of the masonry walls varied on their location (height or storey) within the building, so that it increased from 220 mm at the top of the buildings to 330 mm at ground level, and

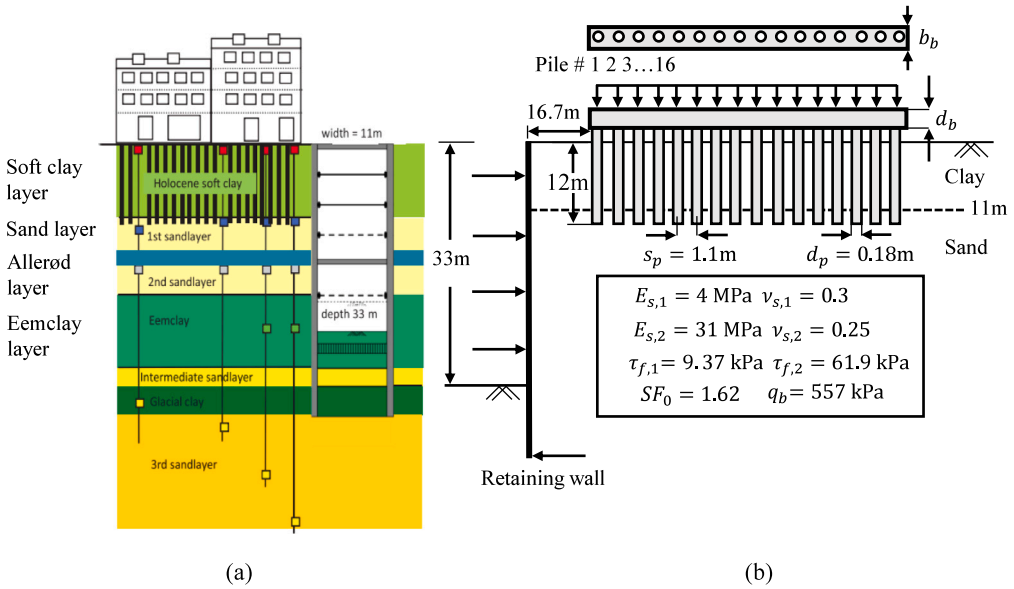

Fig. 7. (a) Cross section of Ceintuurbaan Station with soil profile (Korff et al., 2016); (b) Schematic illustration of building adjacent to excavation in Amsterdam.

reaching 440 mm at the foundation level. For their foundation, the pile embedment length is L_p = 12 m, pile diameter d_p = 0.18 m, and E_p = 8 GPa. As shown in Fig. 7a, the ground stratigraphy at Ceintuurbaan Station is layered. There is a man-made soil fill of 3 m thickness above the soft Holocene clay, and a peat layer (extending to a depth of 11 m), which overlays one dense fine-to-medium sand layer (the "first sand layer", extending to 11.5 – 12.5 m depth) and a heterogeneous layer of sandy clay, clayey sand, and silt ("the Allerød", extending to 25 m depth), followed by a stiff clay layer ("the Eem clay", extending to 50 m depth) and "the 3rd sand layer" (Korff, 2013; Korff and Mair, 2013a).

In the interaction model, greenfield movements were estimated by linearly interpolating monitoring data from Korff et al. (2016) at the surface and at the pile tip depth. The ground model is simplified to a two-layered half-space, similarly to Korff (2013), for which the first layer has thickness $H_{s,1}$ = 11.5 m, $\nu_{s,1}$ = 0.3 and $E_{s,1}$ = 4 MPa, and the second layer has $\nu_{s,2}$ = 0.25 and $E_{s,2}$ = 31 MPa, see Fig. 7b. Piles are modelled as beam elements. The ultimate shaft resistances of the piles are set to $\tau_{f,1}$ = 9.4 kPa and $\tau_{f,2}$ = 61.9 kPa for the two layers, respectively, and the ultimate tip resistance of the piles are set to q_b = 3930 kPa. With these values, the working loads at the pile heads result in a safety factor SF_0 = 1.62 (Korff et al., 2016). The building structure (grade beam and bearing wall) is assumed to be elevated from the ground surface, as mechanically schematised by a beam fixed to the pile heads and having equivalent bending stiffness, EI, ranging between 0.075 GNm^2 and 0.743 GNm^2 (respectively, for the strip foundation alone and the 3 storey wall with openings combined with the strip foundation).

Excavation-induced pile head settlements are analysed in Fig. 8. Monitored pile settlements are compared against results computed using the EP two-stage model with an equivalent beam for the strip foundation alone, or with the building wall resting on the strip foundation; for comparison, greenfield movements at the surface and pile base are also shown. Predicted settlements agree with field data, slightly overestimating the level of the settlement far away from the excavation (e.g., Building 126). The effect of the equivalent bending stiffness EI on the settlement level is nearly negligible, although it affects excavation-induced distortions.

To illustrate this, Fig. 9 evaluates the hogging building distortions for different EI values, and plots the modification factor $M_{hog}^{DR} = DR_{hog}^{bldg}/DR_{hog}^{gf}$ (which normalises the building hogging deflection ratio by the corresponding greenfield value at the ground surface) as a function of the relative bending stiffness parameter $\rho_{hog} = EI/E_s L_{hog}^3$

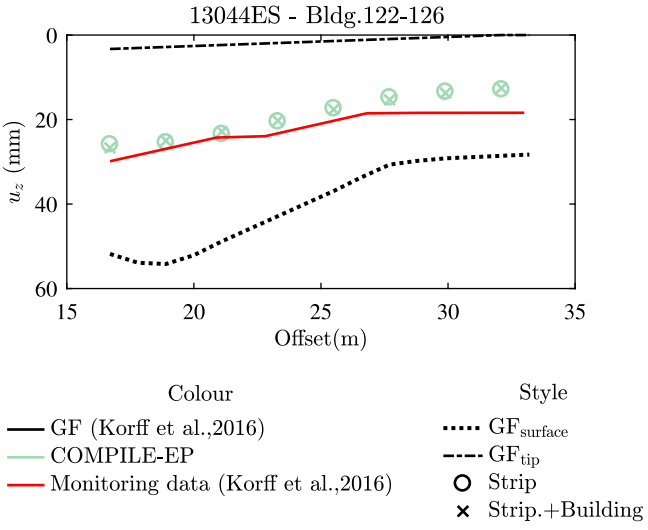

Fig. 8. Comparison with deep-excavation-induced settlements of Buildings 122–126.

(which normalised the superstructure bending stiffness by the foundation stiffness, where E_s is the weighted average of the soil Young's modulus above the excavation level, assumed equal to 18 MPa at the Ceintuurbaan station (Korff, 2013), and L_{hog} is the length of the building in the greenfield hogging zone). Fig. 9 suggests that the interaction model slightly underestimates the M_{hog}^{DR} modification factor values associated with the field data and that the building acted as a rather flexible superstructure, with an equivalent stiffness given by the strip beam alone.

6. Study of vertical and lateral pile responses in layered soil

This section presents a parametric study to illustrate ground and structural aspects that can significantly affect the excavation-induced impact on adjacent deep foundations. These analyses extend the work of Zheng et al. (2021a,b), which were limited to 'floating' piles.

Two deep-excavations designs are considered next to varying structures. Fig. 10 displays all considered scenarios, within which piles are always arranged transversely to the excavation and in a two-layer

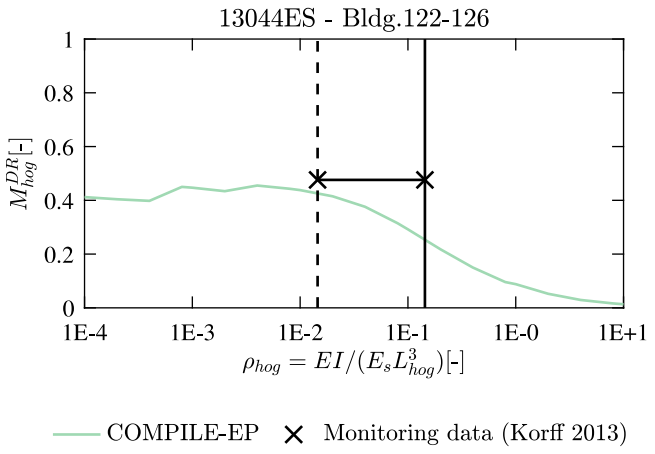

Fig. 9. Modification factors versus relative building stiffness for Buildings 122–126 in the hogging zone.

stratigraphy of clay soil whereas retaining walls reach down to either the pile tip depth ($H_{w,1} = 15$ m) or well below it ($H_{w,2} = 30$ m) for H_w/L_p ratios of 1 and 2, respectively. The excavation affects pile foundations composed of piles having length $L_p = 15$ m, diameter $d_p = 0.5$ m, and Young's modulus $E_p = 30$ GPa: namely, (i) single piles (*SP*; Fig. 10a); (ii) two-pile and four-pile groups (*2-PG* and *4-PG*; Fig. 10b–c); and (iii) piled structures (*PS*; Fig. 10d). All pile groups PG and piled structures PS were also analysed for 'free-head' and 'rigid cap' head conditions. Piles are numbered in progressive order with increasing distance from the wall (e.g., 1–4 for the PS). The offset of the front Pile 1 is set to $X_{p,1} = 3$ m if not specified otherwise; thus, the position of the front Pile 1 in PG and PS analyses is identical to the position of the single pile in SP cases. The spacing between piles is $s_{p,1} = 1.5$ m ($s_p = 3d_p$) and $s_{p,2} = 6$ m ($s_p = 12d_p$) for the pile group (PG) and piled structures (PS), respectively. Table 1 summarises Young's modulus E_{ss} of the beam, tied to the pile heads, used to model three different piles superstructures (PS): a grade beam (GB), a one-storey wall bearing building (B1), and a three storey one (B3). For all superstructures, the service load is $P_0 = 542$ kN and, consequently, different pile vertical capacities Q_{tot} and safety factors $SF_0 = Q_{tot}/P_0$ (within the range 2–3.5) are associated with the three ground conditions (as discussed later).

Three stratigraphies are considered, all with clay soils and with an upper layer thickness of $H_{s,1} = 13.5$ m. They correspond to: (i) a uniform medium-stiffness clay (*sMeMe*), (ii) a very soft upper layer above a stiff bottom layer (*sSoSt*), (iii) a medium-stiffness upper layer above a stiff clay (*sMeSt*). The upper stratum is indicated as Layer 1 ($E_{s,1}$; $\nu_{s,1}$) while the bottom one is Layer 2 ($E_{s,2}$; $\nu_{s,2}$). For the soft, medium-stiff, and stiff clays $E_{s,i} = 1, 16$, and 100 MPa, respectively. For all layers, the following values are considered: Poisson's ratio $\nu_{s,i} = 0.5$, undrained shear strength $c_{u,i} = E_{s,i}/400$, shaft yielding strength $\tau_{f,i} = c_{u,i}$, and ultimate base stress $q_b = 9c_{u,2}$.

Table 2 summarises the three stratigraphies and the corresponding total ultimate capacities (Q_{tot}) of the piles foundation for each case, when ultimate stresses are mobilised. Note that the base capacity (Q_b) is 7% of the total capacity for the sMeMe (uniform) case, 41% for the sSoSt case with a soft upper layer, and 23% for the sMeSt case with the medium upper layer. Also, note that the base-to-total capacity ratio is lower than the ratio P_b/P_0 between the base and head loads inferred from EL analyses of single piles (see Table 2). Thus, piles can be considered as *floating* when embedded in the uniform sMeMe soil, as *intermediate* for the sMeSt case, and as *end-bearing* for the sSoSt case.

Excavation-induced greenfield movements are estimated from Eq. (1) assuming a parabolic deflection for the wall and an average lateral displacement of $0.1\%H_w$.

Table 1
Properties of the beam for the three piled structures PS.

Label	E_{ss} (GPa)	d_b (m)	b_b (m)
GB	30	0.5	0.5
B1	3	0.5	3
B3	3	0.5	9

6.1. Single piles

Single piles (SP) are used to investigate the effect of ground conditions on excavation–pile interactions; analyses conducted considered two wall lengths $H_{w,1} = 15$ m and $H_{w,2} = 30$ m adjacent to 15 m piles, and all three stratigraphies. Figs. 11 and 12 display computed SP results for relatively long ($H_w/L_p = 1$) and relatively short ($H_w/L_p = 2$) piles, respectively; in particular, is shows the excavation-induced vertical and horizontal displacements (u_z^{exc} and u_x^{exc}) the pile axial forces and moments (N^{exc} and M^{exc}); as well as the post-excavation axial force (N^{pos}), shaft friction (τ^{pos}), and horizontal pressure (σ_h^{pos}).

For both excavations, the largest settlements u_z^{exc} in Figs. 11a and 12a are induced in the 'floating' piles embedded in the uniform sMeMe soil, in which the pile–soil interaction along the shaft dominates behaviour, since it provides the largest percentage of shaft capacity in relation to total capacity. Contrarily, 'end-bearing' piles within the sSoSt soil settle less than the other cases, and very close to the greenfield vertical movements at the pile tip level, because their soil–pile interaction is controlled by the stiff bottom layer. Settlements of 'intermediate' piles are bounded by the 'floating' and 'end-bearing' cases. Thus, the ground stiffness profile along the pile controls the resulting settlements.

The largest excavation-induced compressive axial forces N^{exc} are induced in the 'intermediate' case because the sMeSt stratigraphy mobilises the largest τ^{exc} shaft friction and base reaction $N_b{}^{exc}$, whereas the shaft friction τ^{exc} mobilised by the soft soil along the 'end-bearing' pile leads to minimal variation in axial forces N^{pos}. Consistently with Korff et al. (2016), no tensile axial forces N^{pos} occur along the 'floating' or the 'end-bearing' single piles (SP) after the excavation.

Limiting the shaft friction in the EP analyses (as compared to the EL analyses) increased the settlements of all 'floating' and relatively short 'intermediate' piles, whereas it reduced settlements of longer 'intermediate' piles and produced a minimal settlement variation in the 'end-bearing' piles. Also, note that soil yielding ($\tau^{pos} = \tau_f$) occurs at different depths in Figs. 11d and 12d. This happens at the lower and upper parts of the 'floating' and 'intermediate' piles, respectively, where greenfield settlements are smallest and largest. Therefore, soil yielding is not necessarily relevant for 'intermediate' and 'end-bearing' foundations.

Finally, the flexural deflection u_x^{exc} and associated bending moments M^{exc} of 'floating' and 'intermediate' piles are nearly identical, while the displacement profile u_x^{exc} is smoother for the 'end-bearing' piles, hence producing smaller bending moments, as shown in Figs. 11e–f and 12e–f. This is because flexural distortions are controlled by the stiffness of the upper layer, which acts to passively deform the pile through the largest excavation-induced horizontal movement u_x^{exc}, as confirmed by Figs. 11g and 12g in which horizontal reaction stresses σ_h^{pos} are low in the soft clay of the sSoSt case. Overall, bending moments M^{exc} of all single piles (SP) are lower than 60 kNm and, thus, their flexural distortions are modest and the likelihood of lateral soil yielding is negligible when the average lateral displacement of the wall is equal to or lower than $0.1\%H_w$.

Comparing results for the two wall depths considered, it is observed that the vertical and lateral responses are qualitatively similar (compare Figs. 11 and 12), except for the observation that larger settlements are induced by the deeper wall excavation (giving greater compression axial force) and that different greenfield horizontal displacement profiles are produced (but associated with similar pile bending profiles in terms

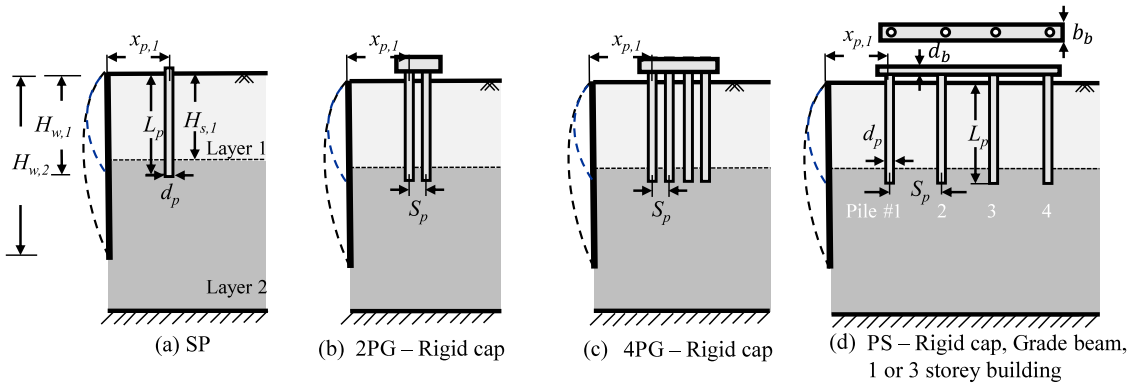

Fig. 10. Parametric study of relatively short ($H_{w,1}/L_p = 1$) and long ($H_{w,2}/L_p = 2$) piles: (a) single piles; (b)–(c) 2 and 4 pile groups; (d) piled structures. Note that, for simplicity, only the deeper wall of $H_{w,2}$ length is shown in the figure.

Table 2
Considered stratigraphies and corresponding pile bearing capacity.

Label	$\tau_{f,1}$; $\tau_{f,2}$	q_b	$Q_r = Q_b/Q_{tot}$	$Q_{s,1}/Q_{tot}$	P_b/P_0 from EL	SF_0
sMeMe	40 kPa, 40 kPa	9 × 40 kPa	7.0%	83.7%	10%	2
sSoSt	2.5 kPa, 250 kPa	9 × 250 kPa	40.8%	4.9%	61.1%	2
sMeSt	40 kPa, 250 kPa	9 × 250 kPa	23.5%	45.1%	32.7%	3.5

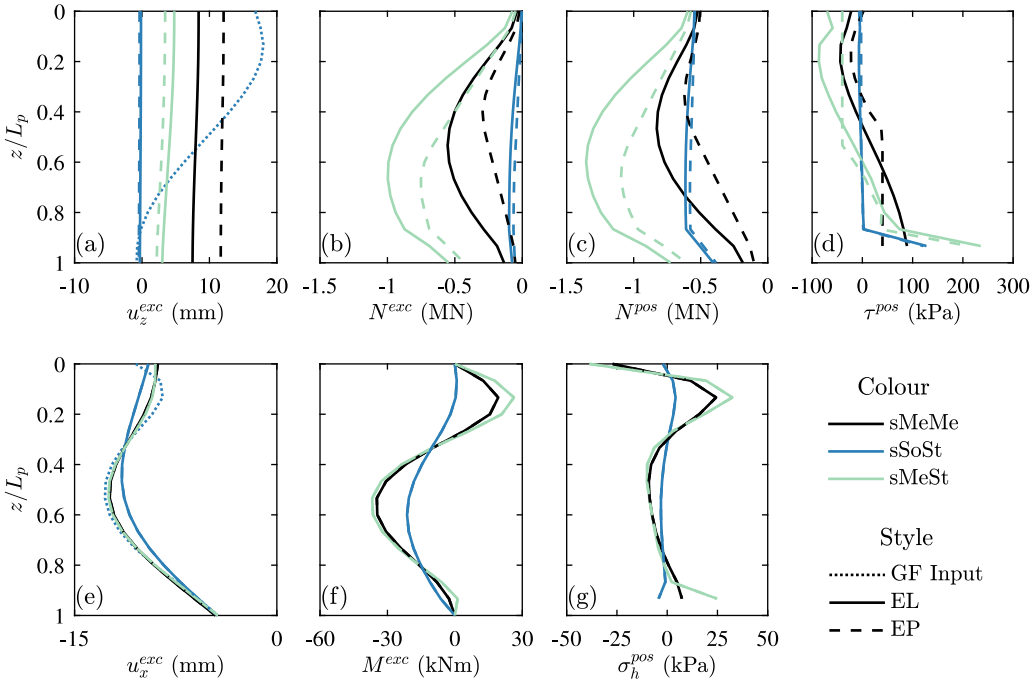

Fig. 11. Analyses of relatively long single pile (SP) for $H_{w,1} = 15$ m ($H_w/L_p = 1$).

of risk assessment). These differences do not play a large role in the distress of single piles SP; however, the influence of H_w/L_P should be considered for capped groups PG and piled structures PS (as later discussed).

6.2. Rigidly capped– and free–head pile groups

This section addresses foundations with a rigid elevated cap, and it compares results with free-head analyses: namely, two pile and four pile groups (2-*PG*; 4-*PG*) and piled structures (*PS*). Figs. 13 and 14 show, respectively for relatively long ($H_w/L_p = 1$) and short ($H_w/L_p = 2$) piles, excavation-induced vertical u_z^{exc} and horizontal u_x^{exc} displacements (including surface greenfield values) and post-excavation axial forces N^{pos} and bending moments M^{pos} along the piles, as computed from the elastoplastic analyses (EP). Also, results for the front Pile 1 are displayed in Fig. 15 for the case with relatively short piles ($H_{w,2} = 30$ m; see supplemental data in Figure S3 for the case with relatively long piles, with $H_{w,1} = 15$ m).

Excavation-induced settlements of free-head pile groups (PG) in Figs. 13 and 14 are smaller than the surface greenfield values and, as it happened with single piles, they vary with the stiffness profile of the ground. Consequently, for all capped foundations considered in the PS and PG analyses, settlements, differential settlements, and slopes between piles are larger for the 'floating' piles than for 'intermediate' and 'end-bearing' piles. Interestingly, different shapes of the settlement profile occur at the free-head group (or fully flexible superstructure) depending on the wall depth H_w and on the soil properties. In particular, purely hogging settlement profiles are associated with both relatively

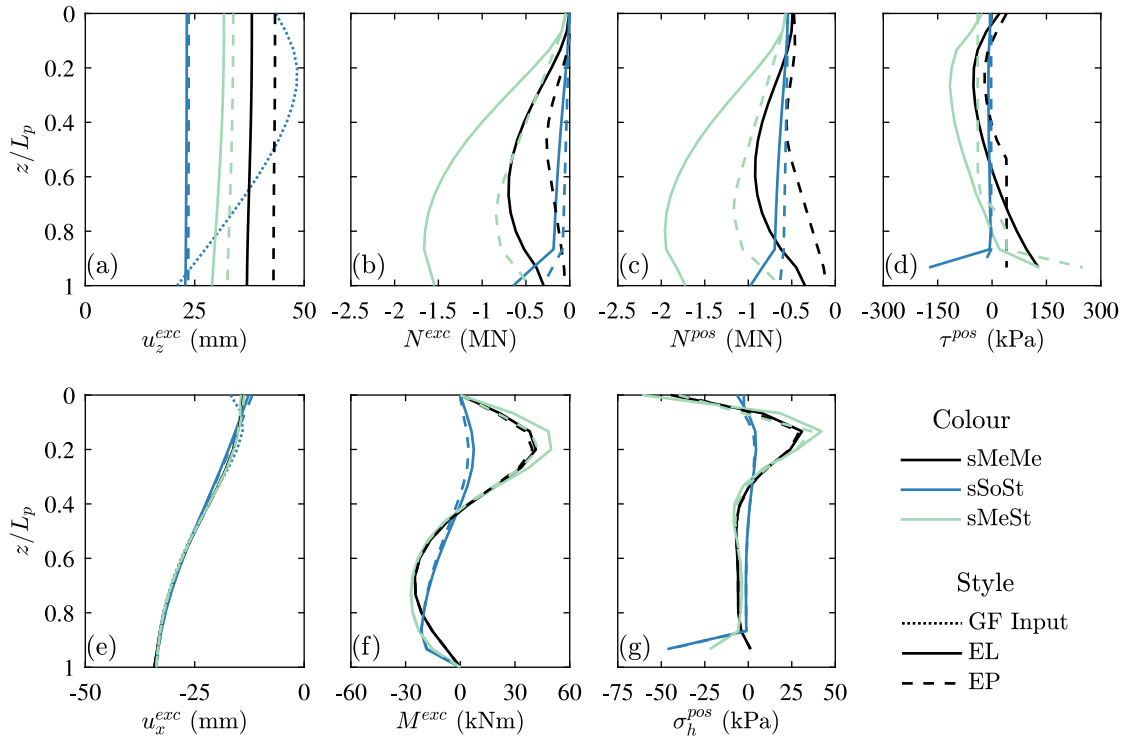

Fig. 12. Analyses of relatively short single pile (SP) for $H_{w,2} = 30\,\text{m}$ ($H_w/L_p = 2$).

short and long 'floating' piles ($H_w/L_p = 1$ and 2). On the other hand, 'intermediate' and 'end-bearing' piles settle with sagging distributions at the relatively long piles ($H_w/L_p = 1$) but they follow hogging profiles for relatively short piles ($H_w/L_p = 2$). The kinematic constrains of the cap causes all pile heads to settle linearly with the horizontal offset, by uplifting/downdragging piles that, under free-head conditions, would settle more/less than the capped group (e.g., for the piled structure (PS) in Fig. 14c, external piles 1 and 4 are uplifted and central piles 2 and 3 are downdragged). In the horizontal direction, free-head horizontal movements u_x^{exc} are similar to the surface greenfield profile, whereas the cap imposes identical horizontal displacements u_x^{exc} of all heads due to its stiffness, that acts by averaging greenfield surface values (see Fig. 14c).

Next, post-excavation axial forces and bending moments are addressed. Note that the post-excavation bending moments at the head node are zero for free-head conditions, while their axial forces are nearly equal to the external service load. In Figs. 13 and 14, the difference in the vertical head forces N^{pos} between free- and capped-heads is due to the kinematic cap action that redistributed axial head forces between piles: downdragged piles are additionally loaded; uplifted piles are unloaded. This vertical load redistribution depends on the ground stratigraphy for all PG and PS foundations: it is greater for the 'floating' than for the 'end-bearing' piles due to larger free-head settlements of 'floating' piles. Despite load redistribution, N^{pos} are compressive following the excavation and, thus, there is a low risk for tensile failure of piles next to excavations.

With respect to flexural distress, bending curvature of piles is caused by the combined cap effect of preventing relative horizontal displacements and imposing identical rotations to all piles (see Fig. 15b). Bending moments M^{pos} in Fig. 15d confirm that, as for tunnel–soil–pile interaction (Loganathan et al., 2001; Kitiyodom et al., 2005), the cap action induces bending moments localised in the upper part of the pile (this mechanism is later discussed for semi-flexible piled structures PS). More importantly, as shown in Figs. 13 and 14, M^{pos} at the pile heads tend to be larger for the 'floating' foundations, particularly for the closely spaced pile groups PG. This is partly due to the larger excavation-induced slope of the foundation leading to cap head rotations being restrained by the lateral soil reaction along the pile. Thus, pile groups with a rigid superstructure may undergo a greater risk of head bending failure for large values of the excavation-induced slope between the pile heads.

Under the assumption of a fixed average wall deflection, wall depths reaching significantly below the pile tip elevation ($H_w/L_p = 2$) increased the detrimental effects on piles, as compared with shallower walls and excavations ($H_w/L_p = 1$). In particular, following greenfield trends, the tilt and settlement of capped piles increased with H_w/L_p leading to larger vertical load redistributions and bending moments within pile groups (e.g., $u_{z,max}^{exc}$ due to $H_{w,2}$ of Pile #1 in 4-PS is 3.63 times the value caused by $H_{w,1}$).

Finally, the influence of soil yielding on pile head displacements and forces is considered. Fig. 16 plots elastic (EL) vs elastoplastic (EP) values for both excavation depths. Considering that ultimate lateral pressures were not reached in the parametric study, limiting the shaft friction in the EP analyses increased significantly the excavation-induced settlements and bending moments only for 'floating' foundations in which the wall length matched the pile tip level ($H_w/L_P = 1$). For the remaining scenarios, when ultimate lateral pressures are not mobilised, linear elastic EL analyses provided results either identical or slightly conservative, as compared with elastoplastic EP analyses. Also, Fig. 16 confirms that ground conditions played a greater role on settlements and bending moments than the role of horizontal movements at the surface level.

6.3. Piled structure

Results for the piled structures PS (including grade beam, one- and three-storey buildings) are compared against analyses for free- and capped-heads to explore the impact of semi-flexible superstructures. Displacements and forces computed at the heads of the piled structures PS are shown in Fig. 17 for the deeper excavation $H_{w,2} = 30\,\text{m}$ ($H_w/L_P = 2$) in uniform soil (sMeMe). This excavation scenario is associated with the largest absolute and differential settlements of the

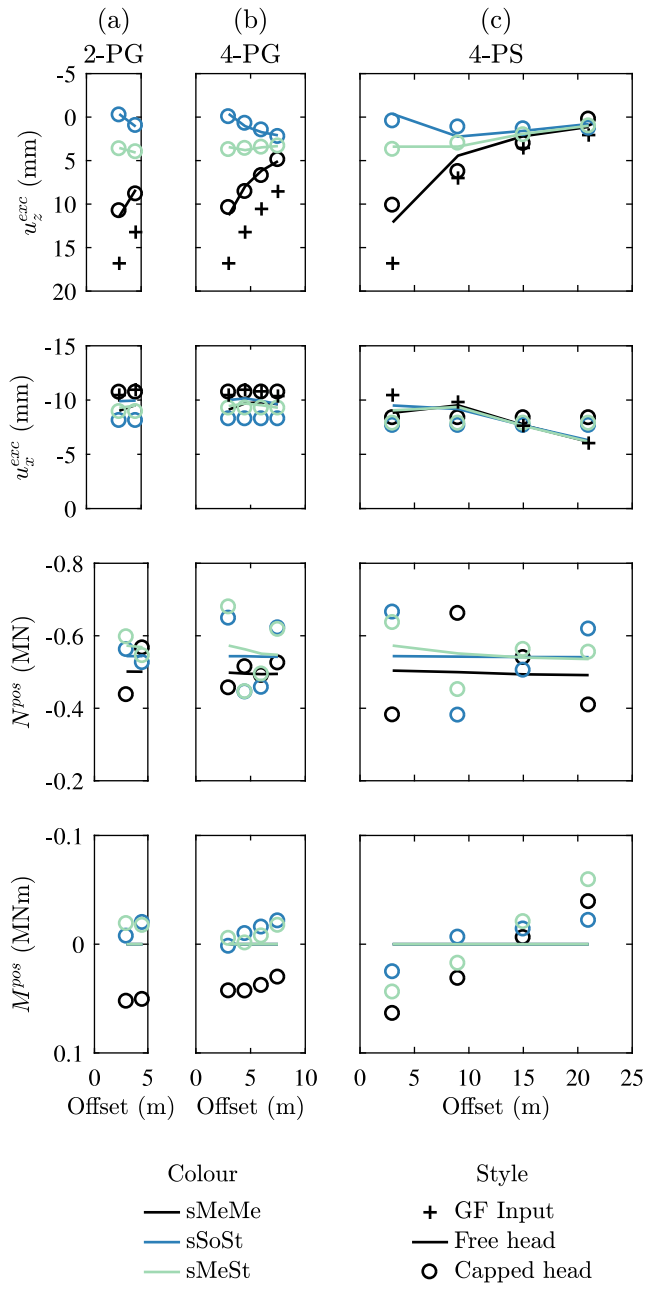

Fig. 13. Excavation-induced movements and post-excavation forces at the pile heads predicted by EP analyses, for relatively long piles with $H_w/L_p = 1$: (a) two pile group; (b) four pile group; (c) piled structures.

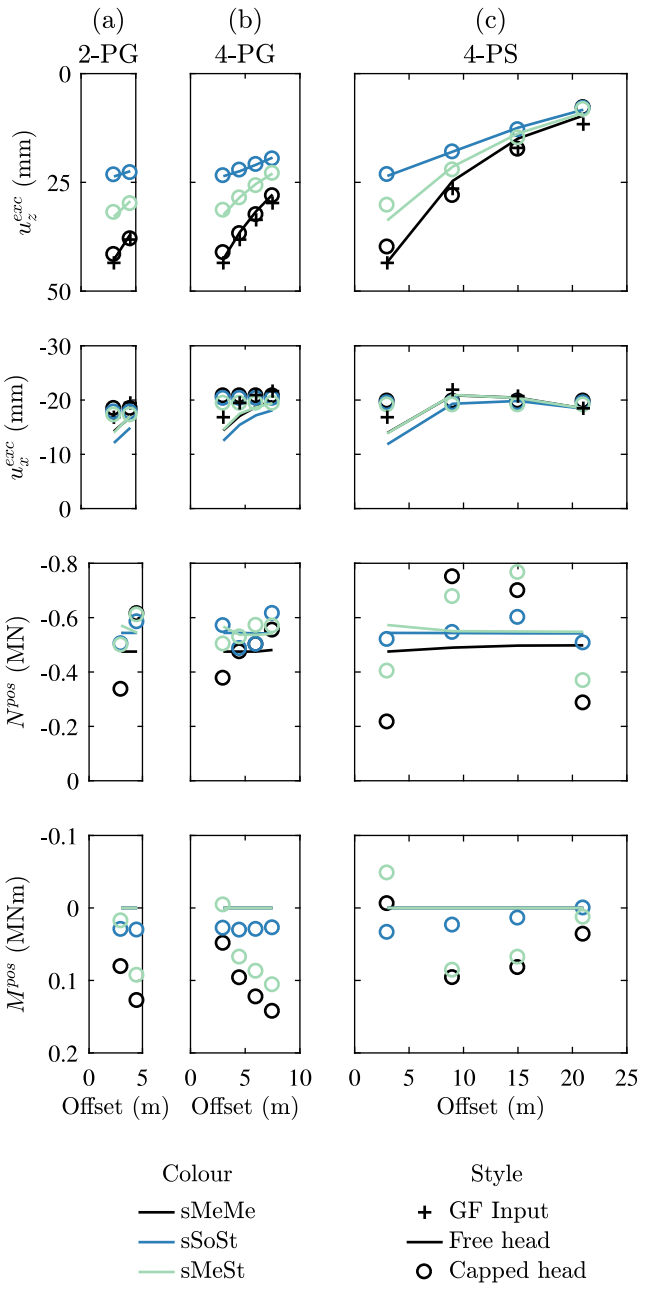

Fig. 14. Excavation-induced movements and post-excavation forces at the pile heads predicted by EP analyses, for relatively short piles with $H_w/L_p = 2$: (a) two pile group; (b) four pile group; (c) piled structures.

free–head PS (see Fig. 14) and, thus, with potential for superstructure deformations. Supplemental Figures S4 and S5 show the subsurface response of Piles #1 and #2, closest to the excavation. Furthermore, Fig. 18a and b show results of the full parametric study (covering all excavation depths and all piled structures); in particular, they show, respectively, the excavation-induced maximum slopes between piles, ω_{max}, and the hogging deflection ratio, DR_{hog}^{bldg}. Fig. 18c and d compare predictions computed with the elastic (EL) and elastoplastic (EP) models.

Fig. 18a shows that increasing the flexural stiffness of the superstructure significantly decreases the maximum slope between piles, ω_{max}, as compared with the case with free-head conditions; also, it reduces the deflection ratio DR_{hog}^{bldg}, as shown in Fig. 18b. Note that the grade beam GB and three-storey building B3 cause distributions of excavation-induced axial forces N^{exc} (and, thus, of maximum slope) that are similar to the free- and capped-head cases, respectively. On the other hand, both the flexible and the stiff superstructures cause bending moments of the pile heads M^{exc} which are about as large as those computed for the rigidly capped-heads, with slightly greater M^{exc} values at the buildings B1 and B3 than at the capped-heads. Thus, although building deformations may decrease with the stiffness of the superstructure, the risk for bending failure of piles should still be assessed for both flexible grade beams and for stiff buildings. Finally, as for rigidly capped-heads, the variation in the axial forces N^{exc} of piles supporting the semi-flexible PS propagates along the pile shafts, whereas the difference in bending moments profiles M^{exc} is localised at the pile heads (see Figures S4 and S5).

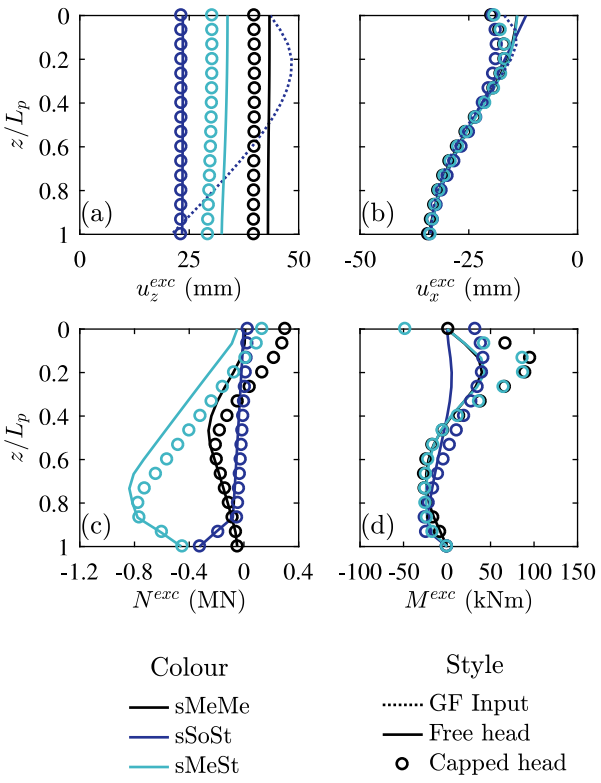

Fig. 15. Responses of Pile #1 within the piled structures PS founded on relatively short piles ($H_w/L_p = 2$) in a two-layered soil with a deep-excavation reaching below the pile tip, $H_{w,2} = 30$ m.

More importantly, Fig. 18a and b show that increasing the building stiffness can minimise the hogging deflection ratio and reduce the excavation-induced slope, ω_{max}, of piled structures with 'floating' piles, whereas the superstructure action has a marginal influence with 'end-bearing' piles. Fig. 18c and d confirm that, as it occurred for capped-piles, linear elastic EL analyses underestimate the excavation-induced maximum slope and hogging deflection ratio of piled structures on 'floating' piles in uniform soil (sMeMe). Finally, when comparing the two excavation depths ($H_w/L_P = 1$ and 2), Fig. 18 shows that extending the deep wall and its excavation below the pile tip level ($H_w/L_P = 2$, as compared to $H_w/L_P = 1$) increases the slope and hogging deflection ratio in all soil conditions, due to larger excavation-induced movements of the ground.

7. Embedment of end-bearing piles

Previous research on excavations close to 'end-bearing' piles seldom considered that their tip may be fully restrained by the stiff bottom layer, and a hinged connection has been often employed. However, this rotational boundary condition may not always be a realistic assumption, as discussed below.

The influence of the embedment length L_e of 'end-bearing' piles into the stiff layer within which the pile tip is introduced is studied next, using elastic analyses (EL) of a relatively shallow excavation relative to the pile length, as shown in Fig. 19. Piles are founded in a bottom layer whose stiffness covers a range from stiff soils to rocks (Young's modulus $E_{s,2}$ of 160 MPa and 16 GPa, respectively). All scenarios differ from the case of Poulos and Chen (1997), because they considered a hinged tip and rigid bedrock at 22 m depth; however, the remaining mechanical parameters are assumed as in Poulos and Chen (1997), as listed in Fig. 19. Fig. 20a and b present excavation-induced horizontal displacements and bending moments for $L_e = 3$ m considering either

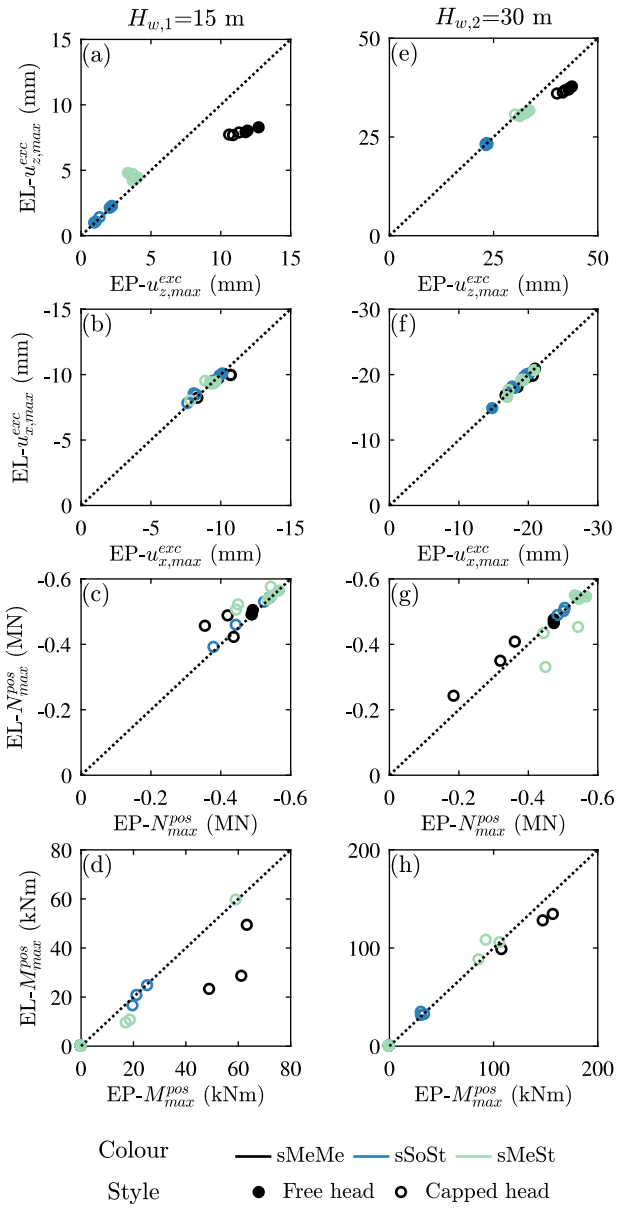

Fig. 16. Comparison of maximum elastic (EL) and elastoplastic (EP) excavation-induced displacements and internal forces at the pile heads: (left) $H_{w,1} = 15$ m, giving $H_w/L_p = 1$ and hence representing relatively long piles; (right) $H_{w,2} = 30$ m, giving $H_w/L_p = 2$ and representing relatively short piles.

stiff clay or rock at the bottom (with $E_{s,2} = 160$ MPa or 16 GPa. Results obtained for different embedments $L_e = [1\,\text{m}; 2\,\text{m}; 3\,\text{m}]$ into the stiff layer are shown in Fig. 20c and d. For comparison, results obtained for the case of no embedment $L_e = 0$ (i.e., hinged condition at the depth of 22 m) are also shown.

As shown in Fig. 20a and c, there are minimal differences in the horizontal displacements u_x^{exc} between cases with and without embedment; such small differences occur around the bottom interface, and are due to the rotational restraint, which is nearly perfect for $L_e = 2$ m in the case of stiff clay ($E_{s,2} = 160$ MPa) and for $L_e = 1$ m in the bedrock ($E_{s,2} = 16$ GPa). More importantly, as displayed in Fig. 20b and d, the partial or perfect rotational restraint led to the development of a bending moment at the interface between both layers, which, in absolute value (signs are different), is about as large as the bending moments at mid-pile depth; bending moments in the upper part of the pile are not affected by the embedment conditions. To achieve a perfect

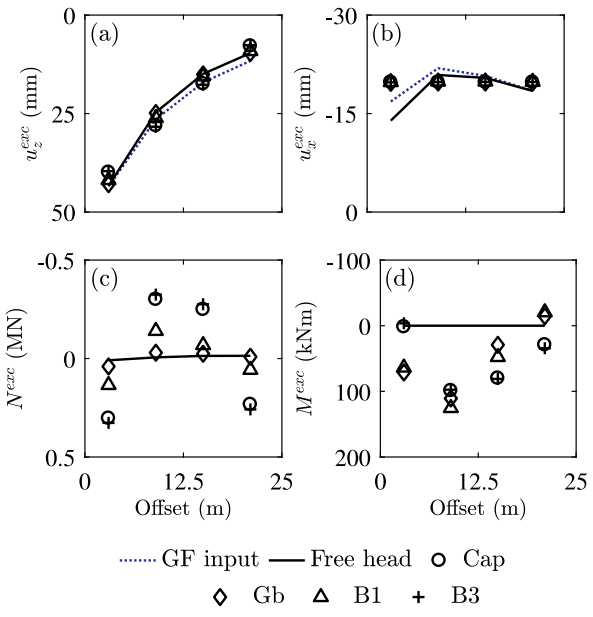

Fig. 17. For the EP analyses, excavation-induced movements and post-excavation forces at the pile heads of piled structures PS in the uniform ground (sMeMe) for $H_{w,2} = 30$ m giving $H_w/L_p = 2$.

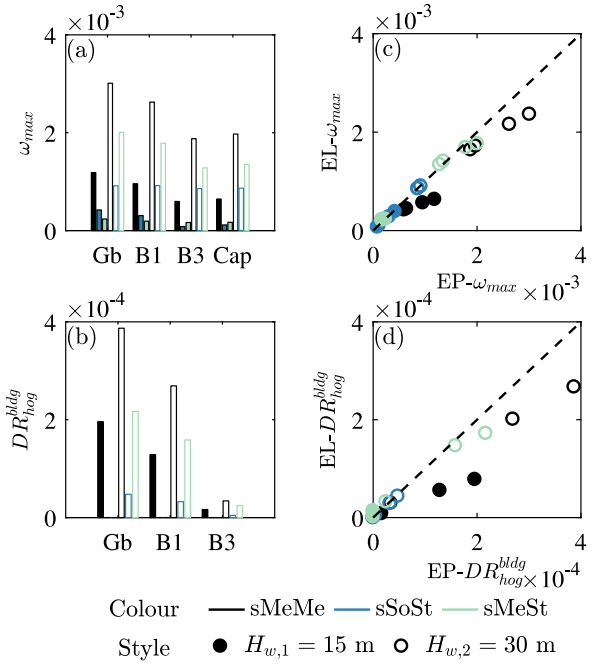

Fig. 18. (a)–(b) Piled structure deformation parameters and comparison between elastic and (c)–(d) elastoplastic maximum values.

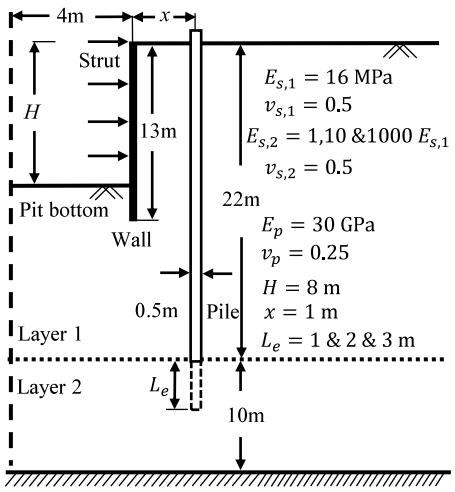

Fig. 19. Configuration and basic parameters of single pile adjacent to deep-excavation.

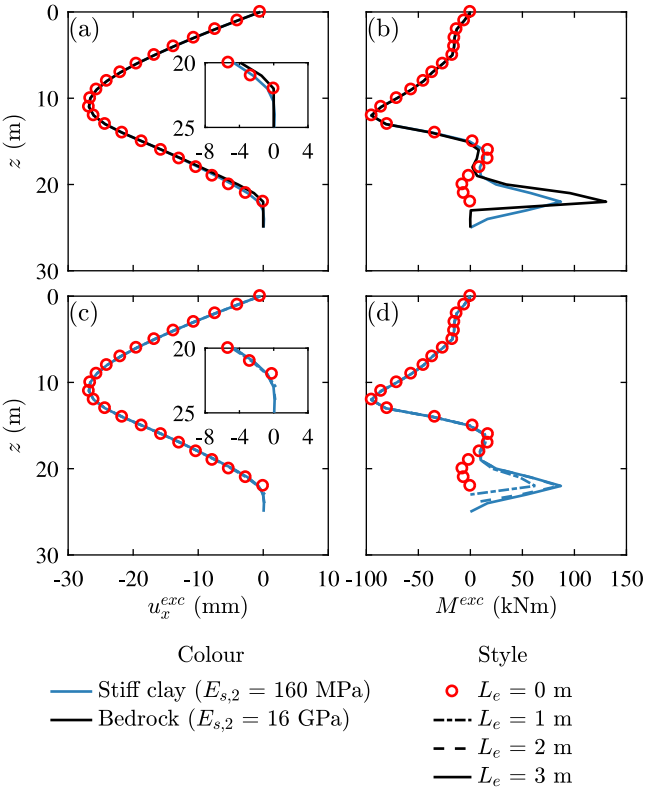

Fig. 20. Elastic response of 'end-bearing' pile with varying embedment conditions in the stiff bottom layer.

rotational fixity, $L_e = 2d_p$ is sufficient when $E_{s,2}/E_{s,1} = 1000$, whereas an embedment length of at least $L_e = 4d_p$ is needed for $E_{s,2}/E_{s,1} = 10$. Partial rotational fixity associated with stiff clay and two diameter embedment ($L_e = 2d_p$; $E_{s,2}/E_{s,1} = 10$) caused bending moments at the interface between layers that are only slightly smaller than those associated with perfect fixity. Therefore, the hinged base modelling is not appropriate when $L_e \geq 2d_p$ and $E_{s,2}/E_{s,1} \geq 10$ (i.e., for most 'end-bearing' pile scenarios), so that fixed base conditions should be adopted for a conservative assessment.

8. Conclusions

This study compares the responses to deep-excavations of a single pile, pile groups and piled structures in layered grounds. The method used is a coupled continuum-based model (COMPILE), which was validated by extensive comparison with analytical, experimental, and field data. Then, an extensive parametric study was conducted to assess the influence of different design variables – wall depth in relation to pile length, ground properties, superstructure stiffness, etc. – on the foundation response. Results indicated that the pile and structural behaviour should be assessed in design by considering the soil–pile–structure interaction and the layered soil condition. Also, fully linear

elastic solutions neglecting soil yielding may underestimate the settlements and bending moments of 'floating' piles, and they may also be inadequate for conservative evaluation of the structural response (slope and deflection ratio). Although the model was validated for different wall deflection shapes, the parametric study is limited to parabolic wall deflection shapes, which are used as a reasonable first approximation for anchored/propped deep-excavations. From this set of analyses, the following conclusions are drawn:

1. Model results confirmed prior knowledge on the response of piles near to deep-excavations in layered soil, and on how such response is affected by the wall depth relative to the pile tip level. 'End-bearing' piles have relatively small settlements, that follow the movements of the base layer, while 'floating' and 'intermediate' piles settle more than 'end-bearing' piles. Also, it was confirmed that, for a given foundation design, larger pile settlements should be expected if the retaining wall extends below the pile tip depth. Novel insights provided by this work are that the occurrence of frictional soil yielding along the shaft (i) plays a minor role for 'end-bearing' piles, (ii) it can increase settlements of 'floating' piles, while (iii) trends are nonlinear for 'intermediate' piles. In contrast, (iv) flexural deformations of piles are controlled by the stiffness of the upper soil layer, where horizontal soil movements are largest, and (v) the effect of lateral soil yielding is negligible in all soil conditions and considered excavations with low wall deflection levels ($\beta = 0.1\%H_w$) nowadays achieved in construction.
2. For both rigidly capped- and free-head pile groups, settlements, differential settlements, and slopes between piles are larger for 'floating' piles than for 'intermediate' and 'end-bearing' foundations. Results from elastoplastic analyses indicated that limiting the shaft friction significantly increased excavation-induced settlements and bending moments only for 'floating' foundations.
3. In relation to the response of capped groups and stiff piled structures to adjacent deep-excavations, the kinematic restriction imposed by the rigid superstructure causes bending moments at the pile heads, while its influence to redistribute the axial head force is limited. Thus, a stiff superstructure may cause bending failure at the head of piles, particularly for large values of excavation-induced slope between piles, while the risk for tensile failure of piles due to nearby deep-excavations is low.
4. For flexible superstructures, deformation modes may depend on both the layered ground conditions and on the relative position of the pile tip with respect to the wall depth, with pure hogging deformation at the pile heads for 'floating' foundations and partly sagging settlement profiles for 'end-bearing' and 'intermediate' piles. When foundations have axially stiff elements connecting pile heads (e.g. grade beams, raft), analyses indicated the risk for bending distress at the pile heads regardless of the bending stiffness of the superstructure due to horizontal greenfield movements varying between piles and the foundation restraining differential horizontal displacements. Also, the interaction model allowed us to evaluate how the bending stiffness of the superstructure affects pile settlements, so that increasing such bending stiffness decreases both the hogging deflection ratio and the excavation-induced slope of 'floating' piled structures, whereas the effect of such superstructure stiffness increase is expected to be marginal on the slope and deflection of 'end-bearing' piles. Evidence was provided that linear elastic analyses combined with free-head conditions employed in previous studies may underestimate the magnitude of pile and structural deformations, especially for 'floating' piles in uniform soil.
5. The parametric study of the influence of embedment length of 'end-bearing' piles into stiff ground or in bedrock illustrated that a sufficient pile embedment length (e.g., greater than two pile diameters into a base layer at least 10 times stiffer) can lead to a partial or perfect rotational restrain of the pile bottom. Thus, modelling 'end-bearing' piles with a hinged base located at the top of the bottom stiff layer is not appropriate: this hinged base modelling neglects the risk for high bending moments concentrating at the interface between soft and stiff layers, which could lead to pile structural failure. Instead, fixed based modelling should be preferred for a conservative assessment.

There are advantages and limitations associated with application of two-stage methods to the problem of deep-excavation effects on piles. One clear advantage is simplicity: in future applications, following the validation in this paper, the proposed two-stage soil–pile-structure interaction model (or similar approaches) could be combined with analytical or numerical methods for estimation of 2D greenfield movements, and then used for the preliminary design of new excavations, bypassing the need for complex 3D numerical models of excavation-soil–pile systems. Possible limitations are (i) that this method neglects the effect of the existing structure, and of its foundation, on the excavation-induced wall deflection; (ii) that the linear elastic half-space theory with constant Young's modulus employed does not consider soil yielding when estimating greenfield movements, and it does not allow one to consider complex patterns of stiffness degradation, associated with shear strain distributions next to the wall and between piles and the wall. Thus, engineering judgement is needed to select the soil's secant Young's modulus to be employed in these models. Furthermore, (iii) variations in effective stress and their effect on pile limit shaft friction and base pressure are not considered. Although this paper extensively validates the practical applicability of the model employed against benchmark physical and numerical results, these fundamental assumptions and their associated limitations should be considered by engineers when the method is employed in practice.

CRediT authorship contribution statement

Chen Zheng: Conceptualization, Software, Validation, Formal analysis, Data curation, Writing – original draft. **Andrea Franza:** Conceptualization, Methodology, Writing – review & editing, Visualization, Supervision, Funding acquisition. **Rafael Jimenez:** Conceptualization, Writing – review & editing, Supervision, Funding acquisition.

Declaration of competing interest

The authors declare that they have no known competing financial interests or personal relationships that could have appeared to influence the work reported in this paper.

Data availability

Data will be made available on request.

Acknowledgements

This project has received funding from the European Union's Horizon 2020 Research and Innovation Programme under the Marie Sklodowska-Curie grant agreement No 793715. Support was also provided by the Spanish Ministry of Science and Innovation, Spain, MCIN/AEI /10.13039/501100011033, Spain, under Grant PID2019-108060RB-I00. The first author also received financial support provided by the China Scholarship Council (CSC) (Scholarship No. 201706930026).

Appendix A. Supplementary data

Supplementary material related to this article can be found online at https://doi.org/10.1016/j.compgeo.2022.105075.

References

Ai, Z., Yue, Z., Tham, L., Yang, M., 2002. Extended Sneddon and Muki solutions for multilayered elastic materials. Internat. J. Engrg. Sci. 40 (13), 1453–1483.

Basile, F., 2014. Effects of tunnelling on pile foundations. Soils Found. 54 (3), 280–295.

Chen, L.T., Poulos, H.G., Loganathan, N., 1999. Pile responses caused by tunneling. J. Geotech. Geoenviron. Eng. 125 (3), 207–215.

Choudhury, D., Shen, R.F., Leung, C.F., 2008. Centrifuge model study of pile group subject to adjacent excavation. In: GeoCongress 2008. (179), American Society of Civil Engineers, Reston, VA, pp. 141–148.

Chow, Y.K., 1986. Analysis of vertically loaded pile groups. Int. J. Numer. Anal. Methods Geomech. 10 (1), 59–72.

Finno, R.J., Bryson, L.S., 2002. Response of building adjacent to stiff excavation support system in soft clay. J. Perform. Construct. Facil. 16 (1), 10–20.

Finno, R.J., Lawrence, S.A., Allawh, N.F., Harahap, I.S., 1991. Analysis of performance of pile groups adjacent to deep excavation. J. Geotech. Eng. 117 (6), 934–955.

Franza, A., Marshall, A.M., Jimenez, R., 2021a. Non-linear soil-pile interaction induced by ground settlements: pile displacements and internal forces. Géotechnique 71 (3), 239–249.

Franza, A., Zheng, C., Marshall, A., Jimenez, R., 2021b. Investigation of soil–pile–structure interaction induced by vertical loads and tunnelling. Comput. Geotech. 139, 104386.

Goh, K.H., Mair, R.J., 2014. Response of framed buildings to excavation-induced movements. Soils Found. 54 (3), 250–268.

Goh, A.T.C., Wong, K.S., Teh, C.I., Wen, D., 2003. Pile response adjacent to braced excavation. J. Geotech. Geoenviron. Eng. 129 (4), 383–386.

Huang, M., Zhang, C., Li, Z., 2009. A simplified analysis method for the influence of tunneling on grouped piles. Tunn. Undergr. Space Technol. 24 (4), 410–422.

Kitiyodom, P., Matsumoto, T., Kawaguchi, K., 2005. A simplified analysis method for piled raft foundations subjected to ground movements induced by tunnelling. Int. J. Numer. Anal. Methods Geomech. 29 (15), 1485–1507.

Korff, M., 2013. Response of Piled Buildings to the Construction of Deep Excavations (Ph.D. Thesis). Cambridge Univ..

Korff, M., Mair, R.J., 2013a. Ground displacements related to deep excavation in amsterdam. In: 18th INternational Conference on Soil Mechanics and Geotechnical Engineering: Challenges and Innovations in Geotechnics, ICSMGE 2013, Vol. 4. pp. 2779–2782.

Korff, M., Mair, R.J., 2013b. Response of piled buildings to deep excavations in soft soils. In: 18th International Conference on Soil Mechanics and Geotechnical Engineering: Challenges and Innovations in Geotechnics, ICSMGE 2013, Vol. 3. pp. 2035–2038.

Korff, M., Mair, R.J., Van Tol, F.A.F., 2016. Pile-soil interaction and settlement effects induced by deep excavations. J. Geotech. Geoenviron. Eng. 142 (8), 04016034.

Leung, C.F., Chow, Y.K., Shen, R.F., 2000. Behavior of pile subject to excavation-induced soil movement. J. Geotech. Geoenviron. Eng. 126 (11), 947–954.

Leung, C.F., Lim, J.K., Shen, R.F., Chow, Y.K., 2003. Behavior of pile groups subject to excavation-induced soil movement. J. Geotech. Geoenviron. Eng. 129 (1), 58–65.

Leung, C.F., Ong, D.E., Chow, Y.K., 2006. Pile behavior due to excavation-induced soil movement in clay. II: Collapsed wall. J. Geotech. Geoenviron. Eng. 132 (1), 45–53.

Liang, F., Yu, F., Han, J., 2013. A simplified analytical method for response of an axially loaded pile group subjected to lateral soil movement. KSCE J. Civ. Eng. 17 (2), 368–376.

Liu, J., Shi, C., Cao, C., Lei, M., Wang, Z., 2020. Improved analytical method for pile response due to foundation pit excavation. Comput. Geotech. 123, 103609.

Liyanapathirana, D.S., Nishanthan, R., 2016. Influence of deep excavation induced ground movements on adjacent piles. Tunn. Undergr. Space Technol. 52, 168–181.

Loganathan, N., Poulos, H., Xu, K., 2001. Ground and pile-group responses due to tunnelling. Soils Found. 41 (1), 57–67.

Mindlin, R.D., 1936. Force at a point in the interior of a semi-infinite solid. J. Appl. Phys. 7 (5), 195–202.

Mu, L., Chen, W., Huang, M., Lu, Q., 2020. Hybrid method for predicting the response of a pile-raft foundation to adjacent braced excavation. Int. J. Geomech. 20 (4), 1–13.

Ng, C.W.W., Wei, J., Poulos, H., Liu, H., 2017. Effects of multipropped excavation on an adjacent floating pile. J. Geotech. Geoenviron. Eng. 143 (7), 04017021.

Ong, D.E., Leung, C.E., Chow, Y.K., 2006. Pile behavior due to excavation-induced soil movement in clay. I: Stable wall. J. Geotech. Geoenviron. Eng. 132 (1), 36–44.

Ong, D.E., Leung, C.F., Chow, Y.K., 2009. Behavior of pile groups subject to excavation-induced soil movement in very soft clay. J. Geotech. Geoenviron. Eng. 135 (10), 1462–1474.

Poulos, H.G., 1989. Pile behaviour—theory and application. GÉOtechnique 39 (3), 365–415.

Poulos, H.G., Chen, L.T., 1997. Pile response due to excavation-induced lateral soil movement. J. Geotech. Geoenviron. Eng. 123 (2), 94–99.

Sagaseta, C., 1987. Analysis of undraind soil deformation due to ground loss. Géotechnique 37 (3), 301–320.

Shakeel, M., Ng, C.W., 2018. Settlement and load transfer mechanism of a pile group adjacent to a deep excavation in soft clay. Comput. Geotech. 96, 55–72.

Son, M., Cording, E.J., 2005. Estimation of building damage due to excavation-induced ground movements. J. Geotech. Geoenviron. Eng. 131 (2), 162–177.

Soomro, M.A., Mangnejo, D.A., Bhanbhro, R., Memon, N.A., Memon, M.A., 2019. 3D finite element analysis of pile responses to adjacent excavation in soft clay: Effects of different excavation depths systems relative to a floating pile. Tunn. Undergr. Space Technol. 86, 138–155.

Tan, Y., Huang, R., Kang, Z., Bin, W., 2016. Covered semi-top-down excavation of subway station surrounded by closely spaced buildings in downtown shanghai: Building response. J. Perform. Construct. Facil. 30 (6).

Tan, Y., Jiang, W., Luo, W., Lu, Y., Xu, C., 2018. Longitudinal sliding event during excavation of feng-qi station of hangzhou metro line 1: Postfailure investigation. J. Perform. Construct. Facil. 32 (4), 04018039.

Xu, K.J., Poulos, H.G., 2000. Theoretical study of pile behaviour induced by a soil cut. In: ISRM International Symposium 2000. International Society for Rock Mechanics and Rock Engineering, Melbourne.

Xu, K., Poulos, H., 2001. 3-d elastic analysis of vertical piles subjected to “passive” loadings. Comput. Geotech. 28 (5), 349–375.

Zhang, R., Zheng, J., Pu, H., Zhang, L., 2011. Analysis of excavation-induced responses of loaded pile foundations considering unloading effect. Tunn. Undergr. Space Technol. 26 (2), 320–335.

Zheng, C., Franza, A., Jimenez, R., 2021a. Coupled elastoplastic analysis of the soil-pile foundation interaction induced by deep excavations. In: Geotechnical Aspects of Underground Construction in Soft Ground. pp. 746–752.

Zheng, C., Franza, A., Jimenez, R., 2021b. A prediction method based on elasticity and soil-structure interaction for deep-excavation induced deformations of pile foundations. In: Challenges and Innovations in Geomechanics. Springer International Publishing, pp. 239–246.